**RESEARCH ARTICLE**

**Key Points:**
- Combined observations give a comprehensive description of the ozone tertiary maximum in the winter polar mesosphere
- Climatological ozone maxima are highest at night in the Northern Hemisphere late winter
- The ozone amount varies interannually in response to varying temperature and vertical transport of $H_2O$ and OH

**Correspondence to:**
A. K. Smith,
aksmith@ucar.edu

# Spatial and Temporal Structure of the Tertiary Ozone Maximum in the Polar Winter Mesosphere

**Anne K. Smith[1]** (iD), **Patrick J. Espy[2,3]** (iD), **Manuel López-Puertas[4]** (iD), **and Olga V. Tweedy[5]** (iD)

[1]Atmospheric Chemistry Observations and Modeling, National Center for Atmospheric Research, Boulder, CO, USA, [2]Department of Physics, Norwegian University of Science and Technology, Trondheim, Norway, [3]Birkeland Centre for Space Science, Bergen, Norway, [4]Instituto de Astrofísica de Andalucía, CSIC, Granada, Spain, [5]Department of Earth and Planetary Sciences, The Johns Hopkins University, Baltimore, MD, USA

**Abstract** Observations from satellites and a ground-based station are combined to construct a global data set for investigating the tertiary ozone maximum in the winter mesosphere for the period August 2004 to June 2017. These give a comprehensive picture of this ozone maximum in latitude, pressure, and time. The location of the tertiary ozone maximum shifts in latitude and pressure with the evolving season; the ozone peak occurs at lower latitude and higher pressure around the winter solstice. Highest average nighttime ozone concentrations and greatest degree of interannual variability are seen in late winter in the Northern Hemisphere (NH). The hemispheric differences and interannual variability in nighttime ozone are related to variations of temperature, $H_2O$, and OH associated with dynamical activity. Elevated stratopause events in the NH winter are associated with transport of air that is depleted in $H_2O$ and enhanced in OH; photochemistry then leads to downward displacement of the altitude of maximum ozone and enhancement in the ozone amount. Transport by planetary waves in the NH extends the region of high ozone further from the pole and leads to longitudinal variations. The analysis shows that while the tertiary ozone maximum responds to a particular radiative situation as shown in previous studies, it is also the result of very dry air found in the winter polar mesosphere.

## 1. Introduction

A seasonally reappearing pocket of high ozone mixing ratio occurs in measurements of the high-latitude winter middle mesosphere around 70–75 km. Marsh et al. (2001) described observations and simulations of this phenomenon, proposed a set of physical processes responsible for its existence, and gave it the name tertiary ozone maximum. Since then, publications have provided a more complete observational record of the morphology and seasonal progression of this feature (e.g., Daae et al., 2014; Hartogh et al., 2004, 2011; Muscari et al., 2012; Sofieva et al., 2009, 2012) and have described processes that perturb the seasonal development.

The mechanism proposed by Marsh et al. (2001) is generally accepted. In winter, the penetration of solar ultraviolet radiation to high latitudes is diminished due to the long optical path through the atmosphere. The formation of the odd oxygen family, Ox, where Ox = O + $O_3$, depends on the photolysis of molecular oxygen, primarily in the Herzberg (195–242 nm) and Schumann-Runge (175–205 nm) bands at this altitude. The loss of Ox is partially due to chemical reaction of atomic oxygen with ozone but, in the mesosphere, is dominated by catalytic cycles involving reactive hydrogen species, HOx, defined as H + OH + $HO_2$. In the vicinity of the ozone tertiary maximum, where HOx lifetimes are short, Ox destruction depends on the renewal of HOx by photolysis of $H_2O$. There is a significant overlap in the spectral range of the radiation that photolyzes $O_2$ and the radiation that photolyzes $H_2O$ (<200 nm). $O_2$ can be photolyzed at longer wavelengths, however, to ~242 nm. The tertiary ozone maximum occurs in a region where the photolysis of $H_2O$ is curtailed relative to the photolysis of $O_2$. In comparison to other latitudes at this altitude, there is then a shift in the balance: Ox production continues while Ox loss due to reactions with HOx species is reduced, resulting in an ozone maximum.

The description of the mechanism proposed by Marsh et al. (2001) emphasizes the role of photolysis in the formation of the tertiary ozone maximum. If photolysis were the only factor involved, the maximum would be symmetric in time around winter solstice, would be nearly identical in the Northern and Southern Hemispheres, and would exhibit no interannual variability except that due to variability in solar ultraviolet radiation. The reality is more complex. Observational studies up to now have documented the ozone response to dynamical events in the Northern Hemisphere (NH; Damiani et al., 2010; Smith et al., 2009;

Sonnemann et al., 2006; Tweedy et al., 2013) and have shown that the seasonal development in the SH is not symmetric about the solstice (see Daae et al., 2014). Observations by Sofieva et al. (2009) also indicate that the latitudinal range of the maximum extends into the polar night where no photolysis occurs.

Ozone and O in the lower to middle mesosphere can be altered by the variable dynamics that are characteristic of the winter middle atmosphere, particularly in the NH, where planetary wave amplitudes can be very large. The NH mesospheric response to sudden stratospheric warmings and elevated stratopause events (Manney et al., 2009) leads to vertical displacement that is first upward during the period of rapid warming in the stratosphere and then downward during the elevated stratopause phase (Kvissel et al., 2012; Siskind et al., 2007; Tweedy et al., 2013). Previous observations have given evidence of an increase in the ozone volume mixing ratio (vmr) at the tertiary maximum during elevated stratopause events (Damiani et al., 2010; Smith et al., 2009; von Clarmann et al., 2013). Several processes could contribute to the perturbations in the maximum ozone vmr and/or the vertical displacement of the ozone layer: vertical transport of ozone itself, transport of atoms or molecules that are involved in the formation or destruction of Ox, or changes in the photochemical balance due to temperature perturbations.

The location and peak concentration of the ozone tertiary maximum can also be perturbed by external forcing. Seppälä et al. (2006), Verronen et al. (2006), Daae et al. (2012), von Clarmann et al. (2013), and Turunen et al. (2016) presented evidence that energetic particles from the Sun or the magnetosphere can affect mesospheric ozone in the vicinity of the tertiary ozone maximum. Interactions of the particles with the atmosphere enhance production of either HOx or NOx (reactive nitrogen, N + NO+NO$_2$). Although both of these families contribute to the catalytic destruction of Ox, only HOx has a strong impact on Ox loss in the polar winter mesosphere. Since the HOx lifetime is fairly short at these levels (hours), its impact on ozone is rapid but short-lived; observations indicate that a response is seen over a period from 1 or 2 to about eight days. Events affecting NH ozone have been documented for January 2005 (Seppälä et al., 2006; Sofieva et al., 2009), December 2006 (Sofieva et al., 2009), January–March 2012 (von Clarmann et al., 2013), and November 2012 (Turunen et al., 2016). An event affecting SH ozone occurred in late July 2009 (Daae et al., 2012).

In this study, we look at the variations of the tertiary ozone maximum due to wintertime dynamical conditions. The emphasis is on monthly timescales and on the relationship between ozone and other dynamical and chemical variables. We use the hemispheric differences, seasonal variation, and interannual variations to better understand the processes responsible for the maximum itself and its variability. As will be shown, the ozone tertiary maximum has both a large diurnal variation and a pronounced seasonal cycle; as a result, no single observational platform is capable of capturing its structure and variability. To achieve the goals of this investigation, we use contemporaneous ozone data from several satellites and a ground-based station to get sufficient information for populating the spatial (longitude, latitude, and pressure) and temporal (time of day, day of year, and interannual) observation grid for ozone. Simulations with the National Center for Atmospheric Research Whole Atmosphere Community Climate Model (WACCM) contribute as a transfer standard to combine observations from different data sets that have discrepancies.

As shown below, this investigation confirms previous findings that the interannual variations in the ozone concentration at the tertiary maximum in the NH respond to strong dynamical perturbations, but we present a more comprehensive survey using 13 years of observations. We also present new results on the longitudinal structure and interhemispheric differences in ozone that are related to variations in the temperature and the concentrations of H$_2$O and OH. We further show that ozone in the NH winter varies substantially with longitude, and we associate this variability with quasi-stationary planetary waves.

## 2. Observational Data and Model Simulations

### 2.1. Ground-Based and Satellite Data

The study relies on observational data from four satellite instruments and one ground-based instrument that sample high-latitude mesospheric mixing ratio of ozone and additional species. In all cases, the individual measurements are made quickly enough that they can be assigned to a specific clock time rather than a longer-term average. Table 1 lists the instruments and some key information about each. The complete names of the instruments and references for ozone observations are British Antarctic Survey Microwave Radiometer at Troll (BAS-MRT; Daae et al., 2014), Michelson Interferometer for Passive Atmospheric

**Table 1**
*Data Used in This Study*

| Instrument | Version | Latitude | Years used | Variables used |
|---|---|---|---|---|
| BAS-MRT | | 72°S | February 2008 to January 2010 | $O_3$ vmr |
| Aura/MLS | 4.2 | 82°S–82°N | August 2004 to June 2017 | $O_3$, $H_2O$, and OH vmr, T, GPH |
| TIMED/SABER | 2.0 | 83°S–83°N | August 2004 to June 2017 | $O_3$ vmr |
| Envisat/MIPAS | V5R O3 m22 | 87°S–89°N | March 2007 to April 2012 | $O_3$ vmr |
| AIM/SOFIE | 1.3 | 25°–90°N and S | May 2007 to January 2017 | $O_3$ vmr |

Sounding (MIPAS; López-Puertas et al., 2018), Microwave Limb Sounder (MLS; Froidevaux et al., 2008), Sounding of the Atmosphere using Broadband Emission Radiometry (SABER; Smith et al., 2013), and Solar Occultation For Ice Experiment (SOFIE; Russell III et al., 2009). In addition to the ozone data, we use MLS observations (Livesey et al., 2017) of temperature, $H_2O$ vmr, OH vmr (Pickett et al., 2008), and geopotential height (GPH). Note that the MLS OH data are only available from 2004 to 2009.

Outliers are removed from each of the data sets. Screening is applied to MLS ozone vmr, temperature, $H_2O$ vmr, OH vmr, and GPH according to the recommendations for each product from https://mls.jpl.nasa.gov/products/. The screening applied to SABER ozone is described by Smith et al. (2013). MIPAS ozone values with averaging kernel diagonal elements smaller than 0.03 have little to no measured information and are therefore not used.

It is evident from Table 1 that observations are not uniform for all years. Although Envisat was launched in 2002, the MIPAS observation modes that included the mesosphere were infrequent in the early years but were applied regularly beginning in 2007. No regular Sun-synchronous observations of mesospheric ozone vmr were available to provide overlapping observations during the first 2.5 years of SABER operations (January 2002 to August 2004). Due to the precession of the TIMED satellite, the local times of SABER observations shift slowly with calendar date. SABER data taken before August 2004 are not used because there are no observations from Sun-synchronous satellites that would enable the local time and seasonal variations to be separated unambiguously. The best coverage for the combined data is obtained for 2008–2012.

## 2.2. Simulations Using WACCM

The specified dynamics option of the Whole Atmosphere Community Climate Model Version 4 (SD-WACCM4) nudges temperature, horizontal winds, and several surface parameters to data from Modern-Era Retrospective analysis for Research and Applications at every model time step. The nudging is applied from the Earth's surface to 50 km and then tapered from 50 to 60 km. Because Modern-Era Retrospective analysis for Research and Applications data are generated by assimilating various meteorological observations, the dynamical fields are close to those observations. SD-WACCM4 can therefore be used to investigate atmospheric composition during specific dynamical events.

SD-WACCM4 simulations using WACCM4 are archived and available for the years 1979–2014 (Morgenstern et al., 2017). Output from the SD-WACCM4 simulations includes profiles along the satellite tracks of the instruments used in this study. With these data, individual biases can be calculated for the model against each of the instruments. The biases computed in this way comprise a large and comprehensive data set because there is a corresponding WACCM profile for every profile from each of the instruments. These biases are used to develop a transfer standard for combining the ozone data from the different instruments. The WACCM simulations are not used otherwise.

## 2.3. Combining Ozone Data From Different Platforms

Several steps are involved in combining data from more than one instrument. To do this, we use the satellite track output mode of SD-WACCM4, described above. All of the observed profiles for ozone are interpolated to the WACCM pressure levels, which have a resolution of about 2.8–3.0 km in the mesosphere. We match up profiles one by one; that is, for each observation profile, we take the WACCM profile that corresponds to it. From these, mean bias profiles for day and for night are computed. Although we found that the biases varied somewhat with latitude and season, this variation appeared to be due to a mix of photochemistry and transport. To minimize the impacts that transport errors in WACCM have on the biases, we do not look at these
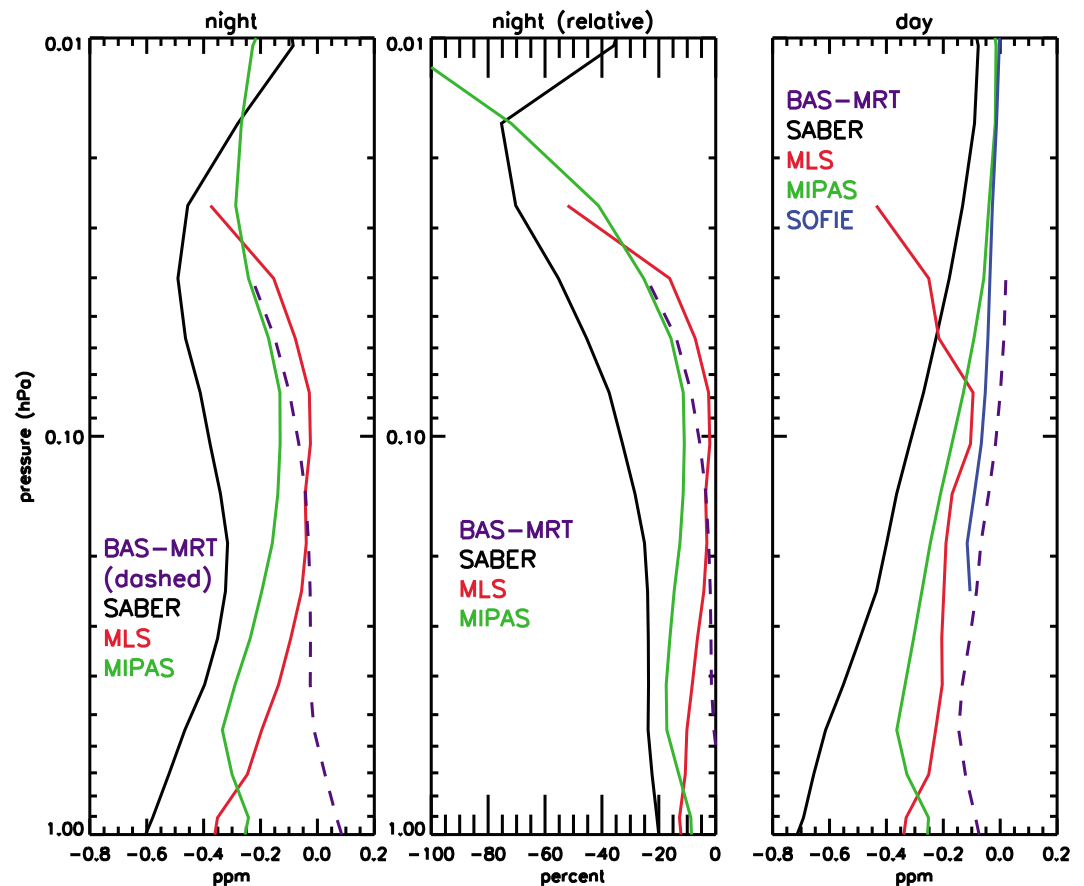
**Figure 1.** Profiles of WACCM biases in ozone mixing ratio against each of the instruments, using model profiles corresponding as closely as possible to the times and locations of the observations. Biases (model minus data) are averaged over all seasons and all available latitudes, separated by night and day. Left is absolute night bias, middle is relative night bias, and right is absolute day bias. Units are ppmv for absolute biases and percent for relative biases.

details but instead compute two ozone bias profiles, one for day and one for night, for each of the instruments. Hourly SD-WACCM4 profiles at the closest grid point to the BAS-MRT location are also available; biases are computed in a similar manner.

Figure 1 shows the bias of WACCM ozone vmr against each of the satellite instruments and against the BAS-MRT ground-based data. The figure shows absolute biases for day and night and relative biases for night. The values are largely negative; WACCM ozone is too low at all altitudes in the mesosphere. The biases of WACCM against the instruments are roughly similar during day and night, and because the overall amount of ozone in this altitude range is higher during night (see Figure 2), the relative biases at night (middle panel) are lower than those during day (not shown). Although the WACCM biases against each individual instrument are based on matched pairs of profiles (WACCM and observations are from the same location, date, and local time), each of the instruments measures under different conditions. These sampling differences could affect the extent to which WACCM simulations agree with the measurements from an individual instrument.

From the bias profiles, we can choose an instrument to use as the "standard" and use each set of instrument-WACCM biases to adjust observations from the other instruments to be compatible. For this, we chose MIPAS as the standard for the following reasons: the mesospheric day and night ozone mixing ratios from the previous retrieval version agree qualitatively with the other measurements evaluated by Smith et al. (2013), the vertical range of the data spans the full altitude range where the tertiary maximum of ozone is seen, and observations during both day and night are available.

The result of combining data will be illustrated using comparisons of ozone variations with local time in the high southern latitudes. Figure 2 shows monthly mean ozone vmr as a function of month and local time at
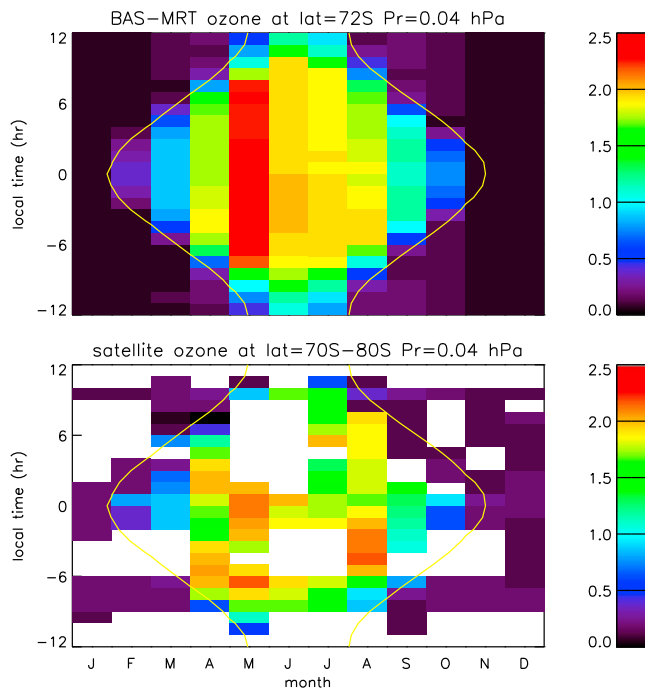
**Figure 2.** Ozone vmr at 0.04 hPa in each month and local time bin for the period February 2008 to January 2010. (top) Ground-based observations from BAS-MRT at 72°S. (bottom) Satellite observations from SABER, MLS, MIPAS, and SOFIE for 70°–80°S. The blank cells indicate local time-month combinations for which no data were available. The yellow lines show the hours when the solar zenith angle was 90°. Units are ppmv. Bias corrections described in section 2.3 have been applied.

0.04 hPa (about 70 km) averaged for the period of the BAS-MRT measurements (February 2008 to January 2010). Results are given for two data sets: ground-based observations from BAS-MRT and the combined data from four satellite instruments for 70°–80°S. Despite the gaps in the satellite coverage, we can see many elements in common between the two panels. The most obvious is the much lower ozone during daytime. Local time hours for which the monthly mean solar zenith angle is close to 90° will have sunlight during part of the hour. These times (indicated by the yellow lines) have monthly average ozone concentrations lower than the nighttime values since they are a mix of day and night. Another feature that is common between the two panels is the rapid increase from low values in daylight to concentrations that vary more with season than with local time. Both panels also indicate that ozone values at this latitude band and pressure are larger before winter solstice than during the midwinter months of June and July. In the further analysis and figures that follow, daytime and nighttime values are averaged separately but local time information is not considered otherwise. Daytime is defined as solar zenith angles less than 90° and nighttime as angles greater than 100°. Daily data are either averaged by month or smoothed with a seven-day running mean, depending on application. Data are sorted and averaged into longitude (20°) and latitude (5°) bins. All analysis is carried out using pressure as the vertical coordinate.

The combined ozone data used in the analysis that follows include the ozone data for the period August 2004 through June 2017. The BAS-MRT data are combined with the satellite data for the appropriate months and longitude and latitude bands. Because there are few observations poleward of 85° in either hemisphere, these latitudes are not included in the analysis.

## 3. Climatology and Variability of the Tertiary Ozone Maximum

As shown in section 2, we can combine various data sources to construct a view of the tertiary ozone maximum that varies with longitude, latitude, pressure, time of day, and day of year. In this section, we show the morphology of that feature and use additional observations to provide evidence for the processes that contribute to the formation of a local maximum in ozone.

Figure 3 gives latitude × pressure cross sections of the zonally averaged ozone for winter months in both hemispheres. Both day and night observations are included in the averages; this is equivalent to taking the zonal average. The ozone maxima are clearly visible in both hemispheres. Highest ozone is located poleward of the average position of the polar night terminator, where most of the profiles used to make the composite data set occur at night. Ozone concentrations reach higher values, on average, in the NH.

### 3.1. Ozone Mean Structure and Seasonal Evolution

It is evident from Figure 2 that the maximum ozone occurs at night. In what follows, we will mainly illustrate the ozone variability using the nighttime vmr. Nighttime values are first sorted into local time bins and then averaged over each local time bin that is filled in an effort to get a reasonable sampling of local times.

Several different projections are shown in order to present a more complete picture of the multiyear average monthly nighttime ozone distribution in time and space. Figure 4 shows the zonally averaged nighttime ozone vmr as a function of latitude × pressure during winter months. This is similar to Figure 3 except that only nighttime values are included. Note that the ozone vmr are larger than in Figure 3 and the latitudes that have high ozone have shifted equatorward, especially in the NH.

Figure 5 shows nighttime ozone as a function of month and latitude at 0.03 hPa. The latitude of the peak ozone follows the location of the polar night terminator. Even though the high ozone values are seen only
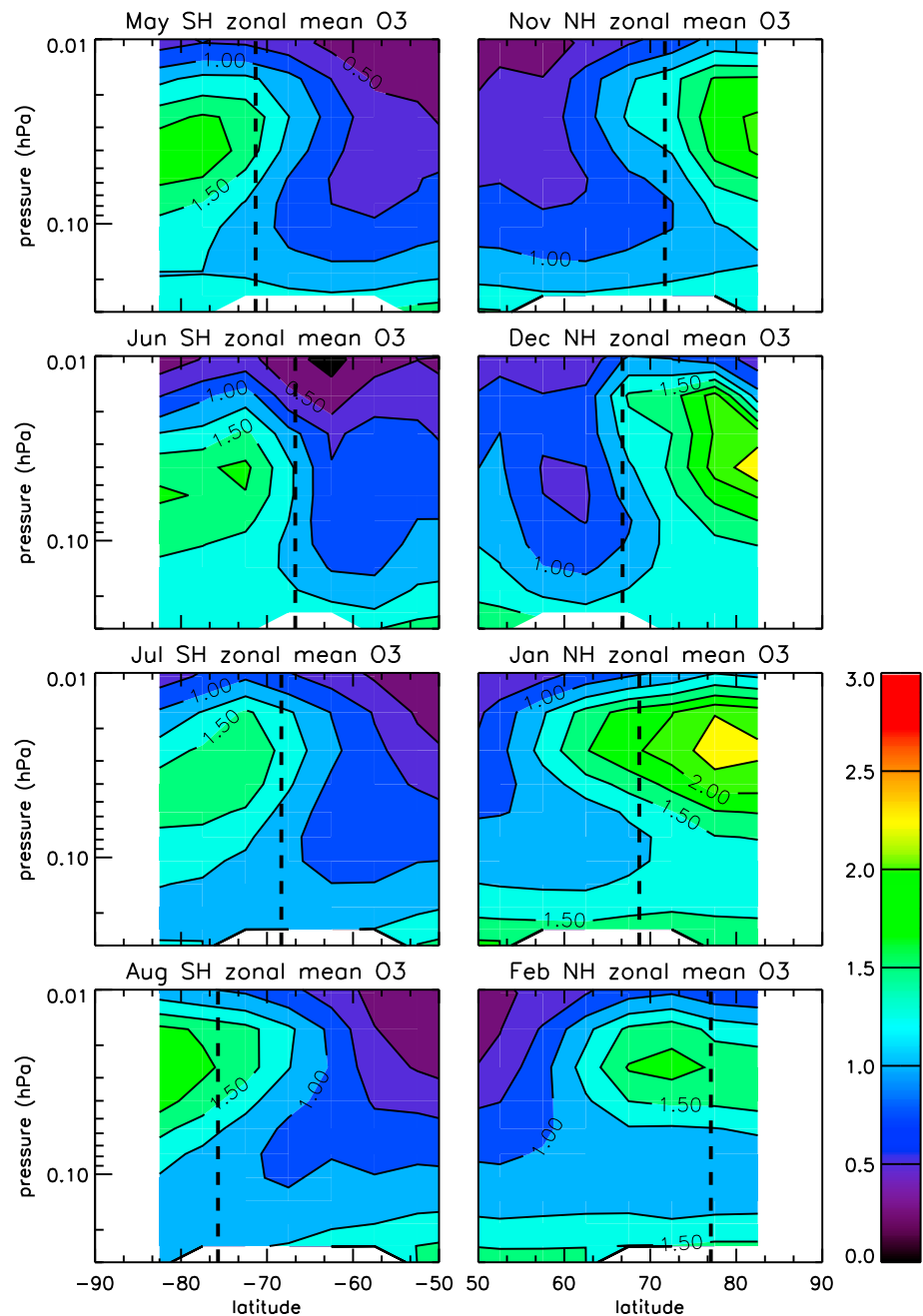
**Figure 3.** Latitude × pressure cross sections of monthly ozone averaged over 2004–2017, including both day and night. Results are shown for latitudes poleward of 50° for winter months. The dashed lines indicate the average position of the polar night terminator. Units are ppmv.

at night, they occur predominately at latitudes that receive illumination during part of the day or that are in close proximity to the edge of the penetration of sunlight. Figure 6 gives nighttime ozone as a function of month and pressure at 70°–75°S and 70°–75°N for winter months in the respective hemisphere.

Figures 4–6 show that the altitude and latitude of the nighttime maxima evolve with season. In the SH, the altitude is lower and the latitude is further from the pole near solstice. In the NH the altitude is higher in early winter and lower in late winter. The maximum value of ozone vmr and the seasonal evolution are different in the two hemispheres. In the SH, maximum ozone vmr occurs in the early winter (see also Figure 2), while the NH has higher ozone in late winter than in early winter.
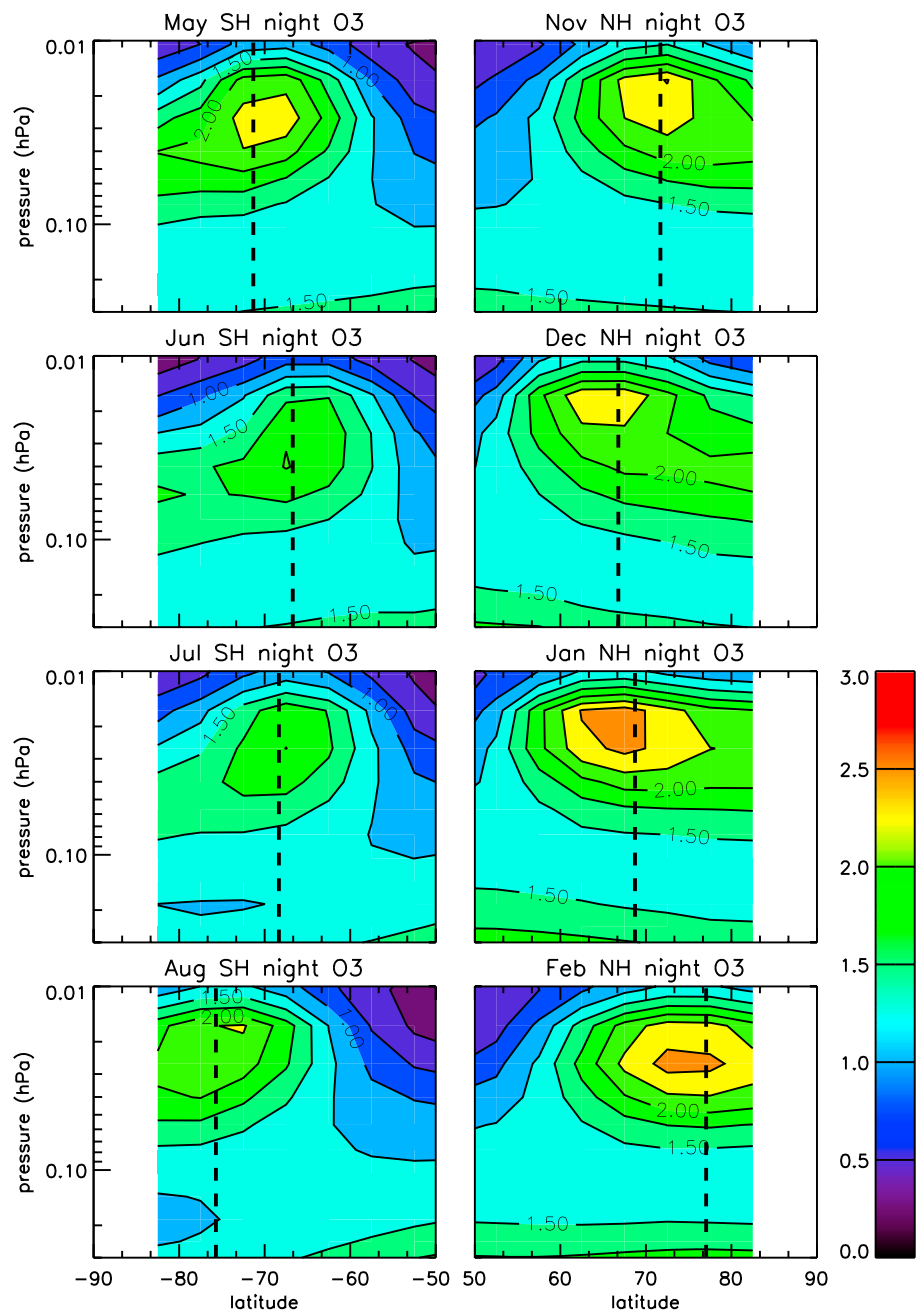
**Figure 4.** As in Figure 3 except showing only nighttime concentrations of ozone. The dashed lines indicate the average position of the polar night terminator.

Figure 7 shows the winter distributions of nighttime ozone and $H_2O$ (day and night averaged) for the latitude bands 70°–80°S and 70°–80°N. This figure uses daily values smoothed with a seven-day running mean. $H_2O$ in high-latitude winter has a fairly long lifetime, and its mixing ratio has sharp gradients in latitude and pressure so its distribution is a good indicator of transport (e.g., Forkman et al., 2005 ; Orsolini et al., 2010 ; Sonnemann et al., 2008). The lowest $H_2O$ mixing ratios are symptomatic of air that has been transported downward from the upper mesosphere.

Comparing the hemispheric differences in the variation of $O_3$ with those of $H_2O$ suggests that the $H_2O$ distribution, in particular the changes during the winter season of the low-$H_2O$ air that indicates downwelling, is related to variations in the ozone. The highest values of average ozone and the lowest values of average
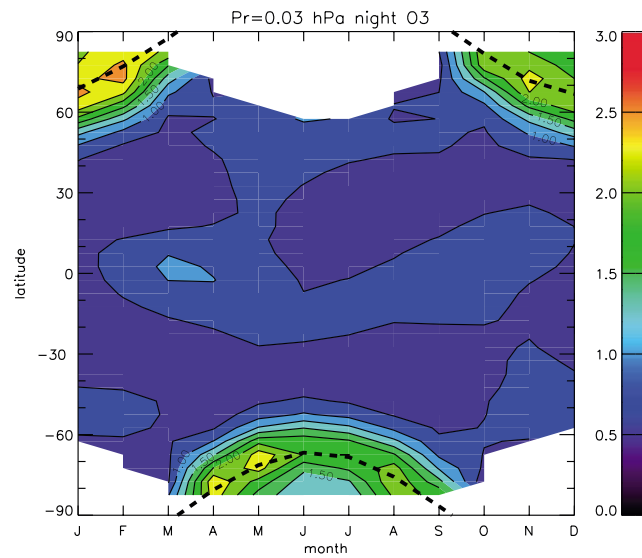
**Figure 5.** Month × latitude cross sections of monthly nighttime ozone at 0.03 hPa averaged over 2004–2017. The dashed line shows the average position of the polar night terminator. Units are ppmv.
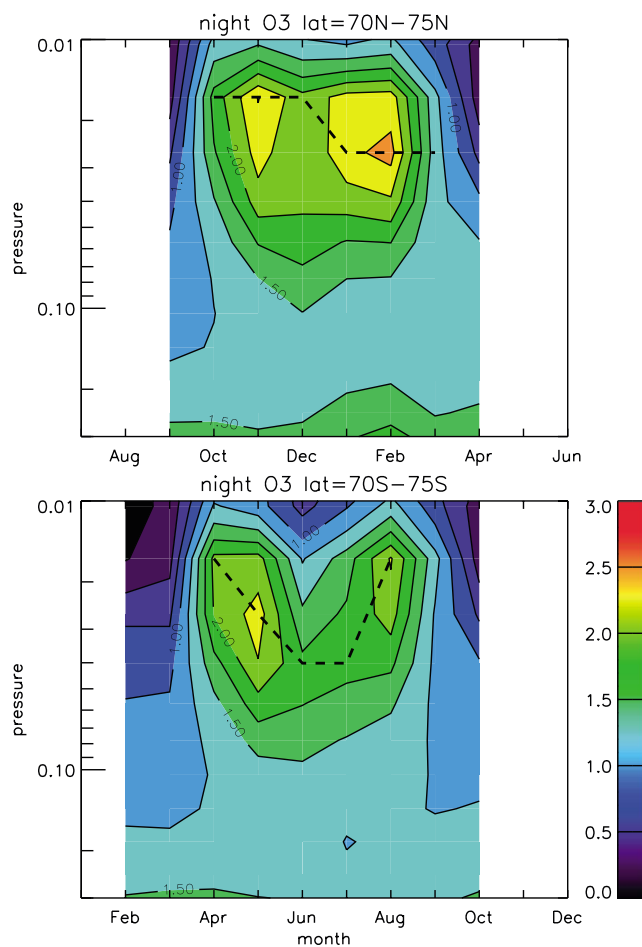


**Figure 6.** Month × pressure cross sections of monthly nighttime ozone for latitudes 70°–75°N and 70°–75°S averaged over 2004–2017. The Northern Hemisphere axis is shifted by six months. The dashed lines show the maximum ozone. Units are ppmv.
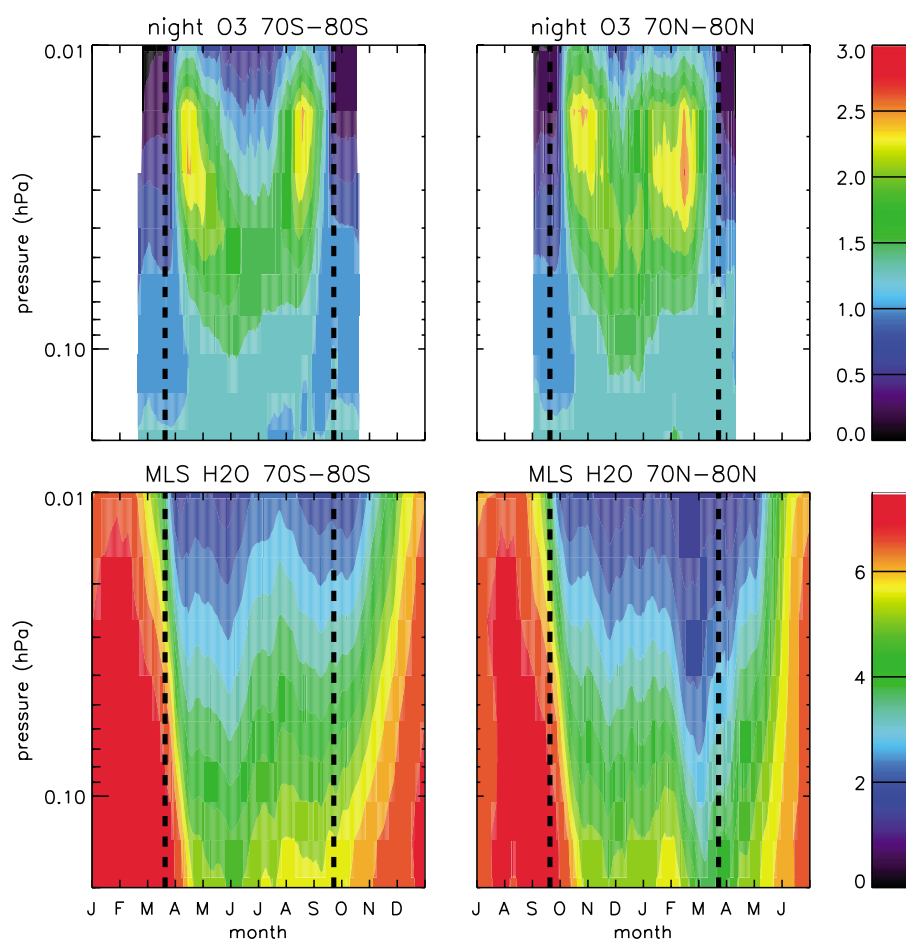
**Figure 7.** Day × pressure cross sections of daily ozone (upper) and $H_2O$ (lower) vmr averaged for 2004–2017 for the latitude bands 70°–80°S and 70°–80°N. Units are ppmv. The dashed lines indicate the times when the polar night begins and ends at 80°S and 80°N.

water occur in April–May in the SH and in February–March in the NH. The variations in $H_2O$ affect the generation of HOx in air that is exposed to sunlight because photolysis of $H_2O$ is the primary source of HOx in this altitude range (Marsh et al., 2001, 2003; Zawedde et al., 2016).

Downward mean circulation can affect ozone in several ways. The adiabatic temperature increase associated with downwelling tends to reduce Ox and also to reduce the $O_3$/Ox ratio due to changes in density and reaction rates (e.g., Smith & Marsh, 2005). Downwelling can also advect HOx from the hydroxyl layer located above the altitude of the ozone tertiary maximum. However, the lifetime of the HOx family decreases rapidly with increasing pressure so it is expected that only vigorous downwelling will bring HOx to 72 km (~0.03–0.04 hPa). Advection of ozone itself cannot generate an isolated maximum. Both ozone and O have short lifetimes around 0.01 hPa (~80 km; e.g., Smith et al., 2010) and, therefore, direct vertical transport of Ox, in the form of either O or $O_3$, is not expected to contribute to the ozone maximum at 72 km. Thus, in summary, the pathway by which downwelling can lead to an ozone enhancement is by a decrease in $H_2O$, which leads to reduced HOx production in air that is exposed to sunlight and therefore reduced Ox loss. In contrast, downwelling can lead to lower ozone by two pathways: both higher temperature from adiabatic warming and advection of air with higher HOx accelerate the photochemical loss of Ox.

### 3.2. Interannual Variations

As seen from Figures 4 and 5, nighttime ozone tends to be high at the latitude of the average polar night terminator. Figure 8 gives profiles of the February mean nighttime ozone for each year in the latitude range of the mean terminator in the NH (70°–75°N). The colors indicate years when there was an elevated stratopause
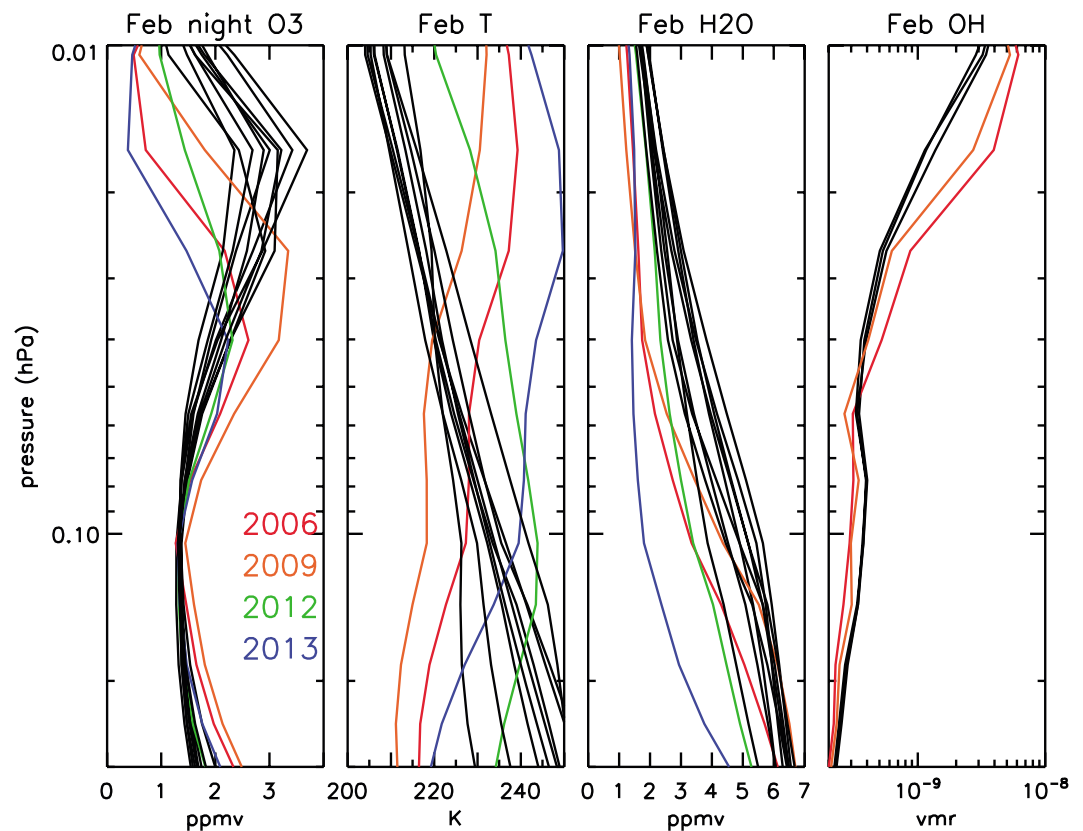
**Figure 8.** Profiles of the February zonal average nighttime ozone vmr (ppmv), temperature (K), $H_2O$ vmr (ppmv), and OH vmr (nondimensional) at 75°–80°N. The ozone, temperature, and $H_2O$ panels include 2005–2017; the OH panel includes 2005–2009. Years for which there was an elevated stratopause event during February are indicated in color.

event in February. The elevated stratopause, characterized by a positive vertical temperature gradient, can be seen in the corresponding temperature profiles. Elevated stratopause events are the result of strong wave-driven downwelling in the mesosphere (Chandran et al., 2013). It is clear from Figure 8 that these four monthlong periods differ quite strikingly from the other nine. The position of the maximum ozone is at a lower altitude during the four elevated stratopause years. $H_2O$ is lower over this pressure range in the elevated stratopause periods, as also documented by Orsolini et al. (2010) for the 2006 and 2009 events. According to the scenarios described above, the reduction in ozone at the upper levels can result from higher temperatures and higher HOx concentrations. Figure 8 shows clear indication of higher T during the four years when elevated stratopause events dominated the February dynamics. The behavior of HOx can be seen in the OH profiles for February of 2005–2009. The larger ozone seen around 0.04–0.05 hPa in elevated stratopause winters occurs in a pressure range where the concentrations of $H_2O$ are lower and temperature is higher. The OH concentration in elevated stratopause years (2006 and 2009) varies with decreasing altitude from higher than that seen in other years (2005, 2007, and 2008) to lower over the pressure range where the ozone maximum occurs.

Figure 9 shows the latitude × pressure cross sections of NH nighttime ozone averaged over Februaries with elevated stratopause events (referred to as active winters), those without (referred to as quiet winters), and the percentage differences. Average (day and night combined) temperature and vmr of $H_2O$ and OH as measured by MLS are also shown. During the active winters, the location of the ozone maximum ozone is at a lower altitude, as already seen in Figure 8. The maximum is also shifted to lower latitude and appears on the equatorward side of the mean position of the polar night terminator. The OH concentration is higher during active winters in the upper part of the range shown, as also shown by Damiani et al. (2010). At polar latitudes, the positive perturbation of OH in active winters extends through all pressure levels shown although the magnitude decreases in the lower levels. Moving further from the pole, the OH perturbation shifts from positive to
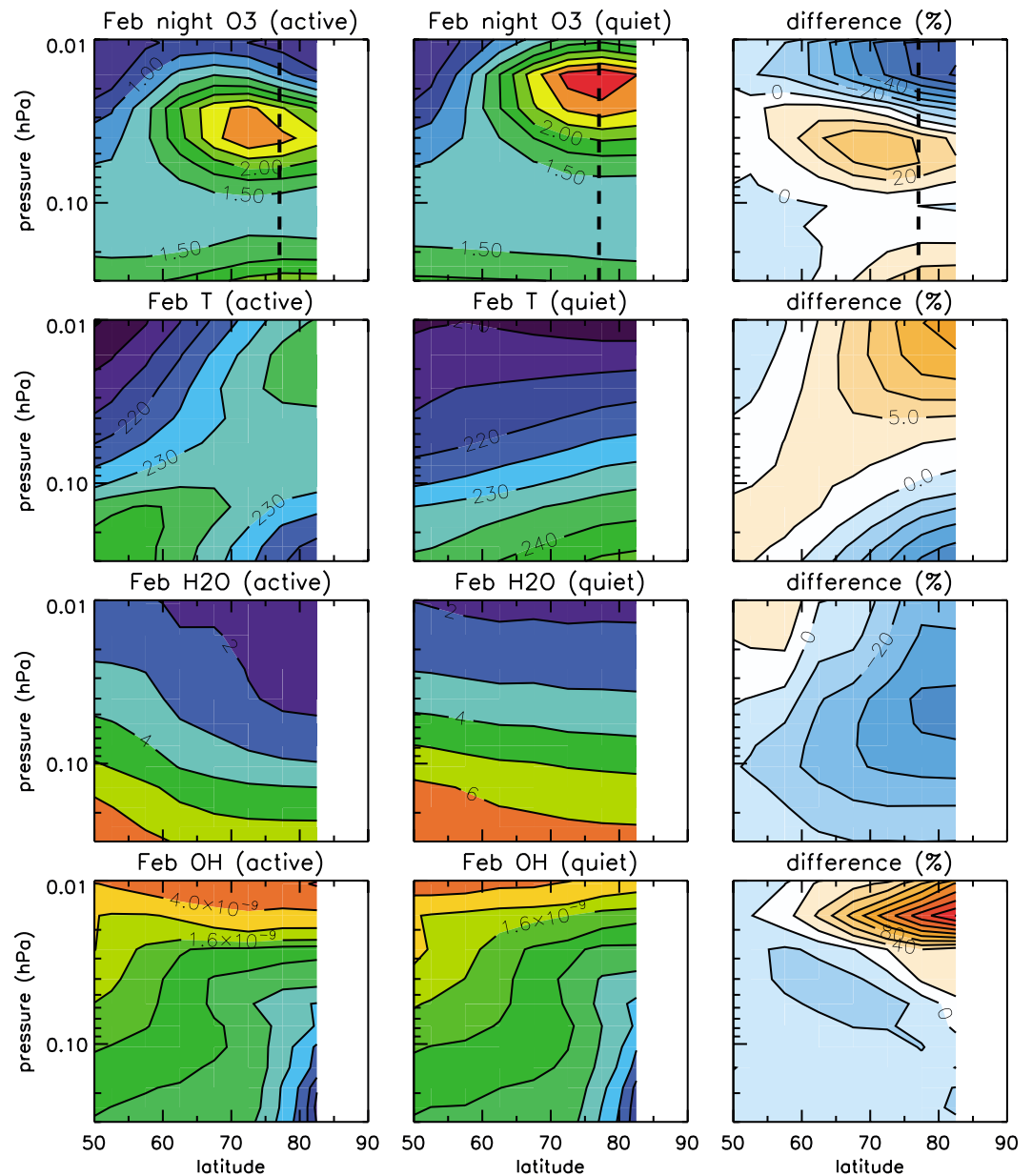
**Figure 9.** Latitude × pressure cross sections of February nighttime ozone vmr (ppmv), temperature (K), $H_2O$ vmr (ppmv), and OH vmr (nondimensional). Ozone, temperature, and $H_2O$ are averaged over 2005–2017; OH is averaged over 2005–2009. Panels in the left column ("active") include 2006, 2009, 2012, and 2013. Panels in the center column ("quiet") include all other years within this period. Right panels show the percentage difference. The dashed lines in the top panels indicate the average position of the polar night terminator.

negative at progressively higher altitudes. The higher OH during active periods is consistent with stronger downward advection from the hydroxyl layer above. The coincidence of higher OH, higher temperature, and lower ozone above about 0.02 hPa indicates that the ozone in the 0.01–0.02 hPa pressure range is reduced in elevated stratopause periods due to the enhanced destruction by the Ox-HOx chemical reactions.

In the years with elevated stratopause, the ozone maximum is apparently displaced in the vertical. As noted above, the photochemical lifetimes of O and $O_3$ are short. For example, the lifetime of O against the reaction O + OH, calculated for the temperature and OH during these winters, is about 12 hr (not shown). The vertical transport velocity estimated by Siskind et al. (2007) from observations during the active 2006 winter is 10 km in 2 weeks, or about 0.7 km/day. The displacement of the maximum is therefore not due to downward
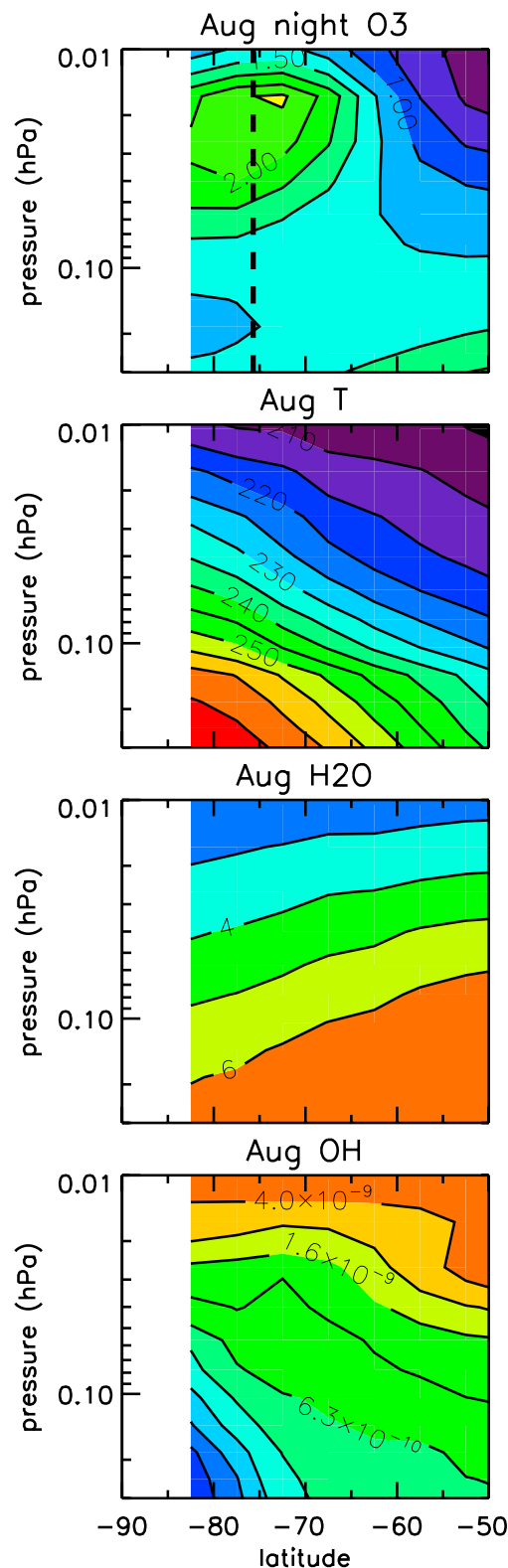
**Figure 10.** Latitude × pressure cross sections of August nighttime ozone vmr (ppmv), temperature (K), H₂O vmr (ppmv), and OH vmr (nondimensional). Ozone, temperature, and H₂O are averaged over 2004–2016; OH is averaged over 2004–2009. The dashed lines in the top panels indicate the average position of the polar night terminator.

advection of Ox by the downwelling circulation. Instead, the maximum forms at a lower altitude and lower latitude where the OH concentration is reduced (Figure 9).

For a comparison with the situation during SH winter, Figure 10 shows the night ozone, and averaged temperature and H₂O for all August periods (2004–2016) and the averaged OH for 2004–2009. There were no SH August cases that corresponded to the "active" NH periods with elevated stratopause so all SH years are grouped together. The ozone is lower and the temperature and H₂O vmr are higher than those in both quiet and active NH winters. SH August averaged OH shows higher vmr near 0.001 hPa, in common with the active February NH conditions, but the SH OH vmr does not decrease as rapidly with increasing pressure. Both the higher OH and the higher temperature are consistent with overall lower ozone vmr at the tertiary maxima in the SH compared with those in the NH.

To look further at the equatorward displacement of the ozone tertiary maximum during active NH winters, Figure 11 shows GPH, temperature, and the mixing ratios of nighttime ozone and day and night H₂O on the 0.03 hPa pressure level for February 2012. This was an active month with an elevated stratopause that followed a stratospheric sudden warming in January (see Figure 8). The contours of GPH coincide approximately with the streamlines for horizontal airflow. The presence of a planetary wave with wavenumber 1 can be seen in the GPH field. The temperature also varies in association with the same wave; the temperature phase is shifted in longitude from that of the GPH. The H₂O vmr distribution follows the planetary wave and reaches its lowest value in the center of the polar vortex, where the GPH is also low and the temperature is high. Ozone also shows a wavenumber 1 distribution in longitude. The ozone maximum (~270°E) is located near the longitude where H₂O reaches a minimum and temperature reaches a maximum at this latitude.

Figures 9 and 11 suggest that two factors contribute to the equatorward shift of the ozone maximum. One is the presence of air with very low H₂O vmr in high latitudes, which is a result of strong downwelling associated with the elevated stratopause event. The other is the presence of a planetary wave that moves the dry air further away from the pole at some longitudes. The amount of HOx produced when that air is exposed to sunlight is lower. There is in general an increase in HOx concentration with increasing distance from the winter pole that occurs due to increasing day length (Figures 9 and 10). This pattern is modified by the extreme dryness. In effect, the transport by planetary waves leads to longitude sectors with very low H₂O, low HOx production, and therefore reduced destruction of Ox and ozone. This is supported by Figure 12, which shows the longitude × latitude distributions for February 2009. This month also had very dry air in the polar region due to an elevated stratopause event. However, during February the quasi-stationary planetary wave amplitudes were not large. The ozone vmr is high, but consistent with the weaker wave motion, the maximum ozone concentrations are seen in the vicinity of the terminator rather than at more equatorward latitudes. For this month, the longitudinal distribution of ozone is much more zonally uniform than that during February 2012 (Figure 11). The meridional transport by planetary waves can also move air from lower latitudes into the
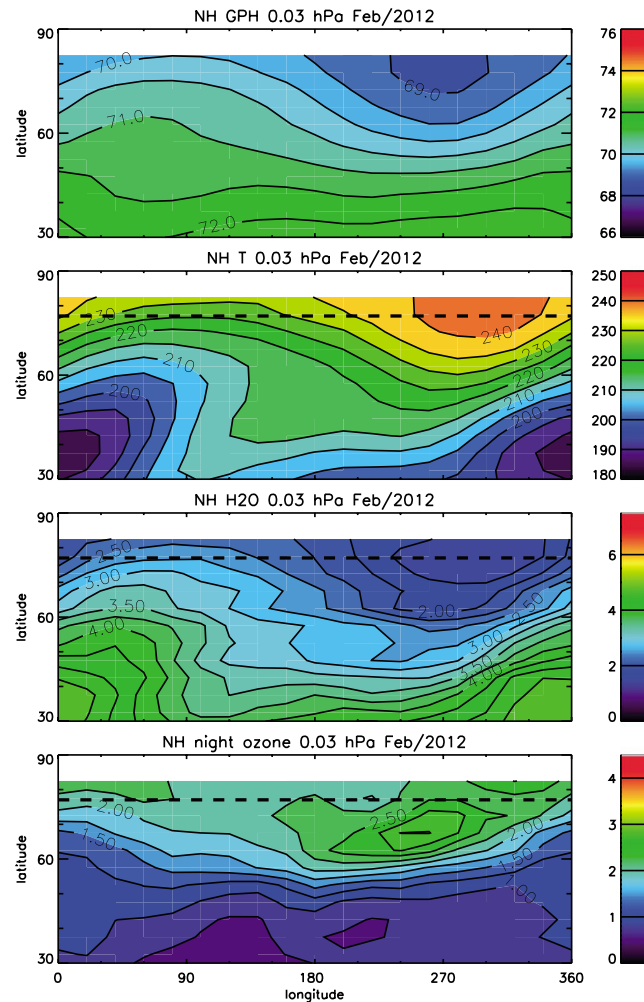
**Figure 11.** Longitude × latitude cross sections of geopotential height (km), temperature (K), $H_2O$ vmr (ppmv), and nighttime ozone vmr (ppmv) at 0.03 hPa in the NH for February 2012. The dashed line gives the average February position of the polar night terminator.

polar region. By this mechanism, air from lower latitudes that has enhanced OH can contribute to ozone loss near and poleward of the polar night terminator.

Figure 13 shows scatter plots of several monthly mean perturbation quantities (deviations from the zonal average) for the latitude band 70°–75°N during February and 70°–75°S during August: ozone versus $H_2O$, $H_2O$ versus temperature, and ozone versus temperature. The points in each panel represent 18 longitude bins and 14 years. All observations are for 0.03 hPa. Figures 9 and 11 indicate that for 70°–75°N in February, low $H_2O$ coincides with higher ozone. However, Figure 13 shows only a weak hint of an anticorrelation between ozone and $H_2O$ for February when the perturbations are relatively large, that is, when planetary wave amplitudes are large. Based on photochemistry, mesospheric ozone is expected to be higher when temperatures are lower, but this expected negative correlation is not seen. The negative correlations of $H_2O$ with temperature (middle column) are strong and consistent with expectations since both respond strongly to vertical motion. An explanation for the low correlations of ozone with either temperature or $H_2O$ is that these two factors are counteracting one another; lower $H_2O$ (predicting lower HOx and therefore higher ozone) is normally seen in phase with higher temperature (predicting lower ozone). For February in the NH, the impact of $H_2O$ variations appears to be very weakly dominant but only because of very large perturbations in $H_2O$. Note that the MLS-Aura OH data are available for only some of the years and are somewhat noisy in longitude so they are not included in Figure 13. The comparable panels for the SH
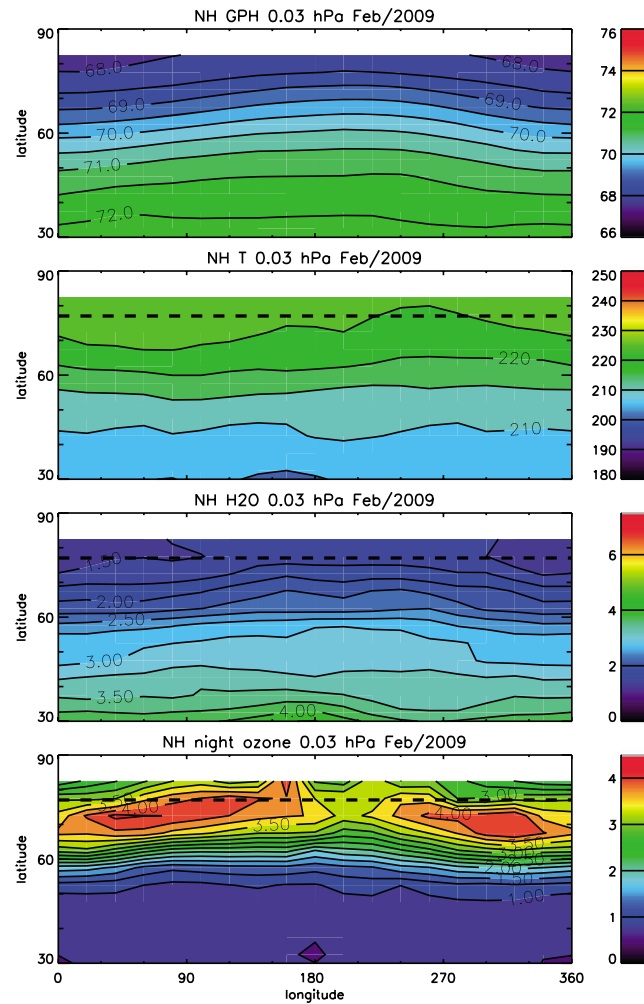
**Figure 12.** As in Figure 11 but for February 2009. The dashed line gives the average February position of the polar night terminator.

(bottom row) show smaller ranges of variation in all three quantities. The anticorrelation between ozone and temperature that is predicted by photochemistry is clearly evident. The temperature effect dominates over the impact of $H_2O$, in contrast to the pattern in the NH. The positive correlation between ozone and $H_2O$ that is apparent in the SH can be explained as a result of the dominance of temperature on the equilibrium ozone, along with the strong dynamically driven correlation between $H_2O$ and temperature. Note that this is not because temperature perturbations are higher in the SH; they are not. However, the SH case has overall higher mean values of $H_2O$ near the pole (compare Figures 9 and 10) and, in addition, is lacking large positive and negative perturbations in $H_2O$ concentration that are seen during some periods in the NH. These factors indicate that the weaker perturbations in $H_2O$ account for the weaker response of ozone to $H_2O$.

The basic concepts of the Marsh et al. (2001) mechanism are consistent with these observations. Near the terminator the production of HOx from $H_2O$ is reduced due to the long pathlength of incoming radiation, thereby reducing ozone loss. At the same time the production of O during the day, which recombines into $O_3$ at night, continues. This results in a region of enhanced ozone near the terminator. The enhanced ozone is seen in all winter months and in both hemispheres, regardless of the level of dynamical activity. However, the concentration of $H_2O$ in the polar region is highly variable due to the transport of air with very low $H_2O$ air during perturbed NH winter periods. Strong planetary waves can transport air with low $H_2O$ out of the polar region at some longitudes, resulting in longitudinal variations in the production of HOx and therefore in the
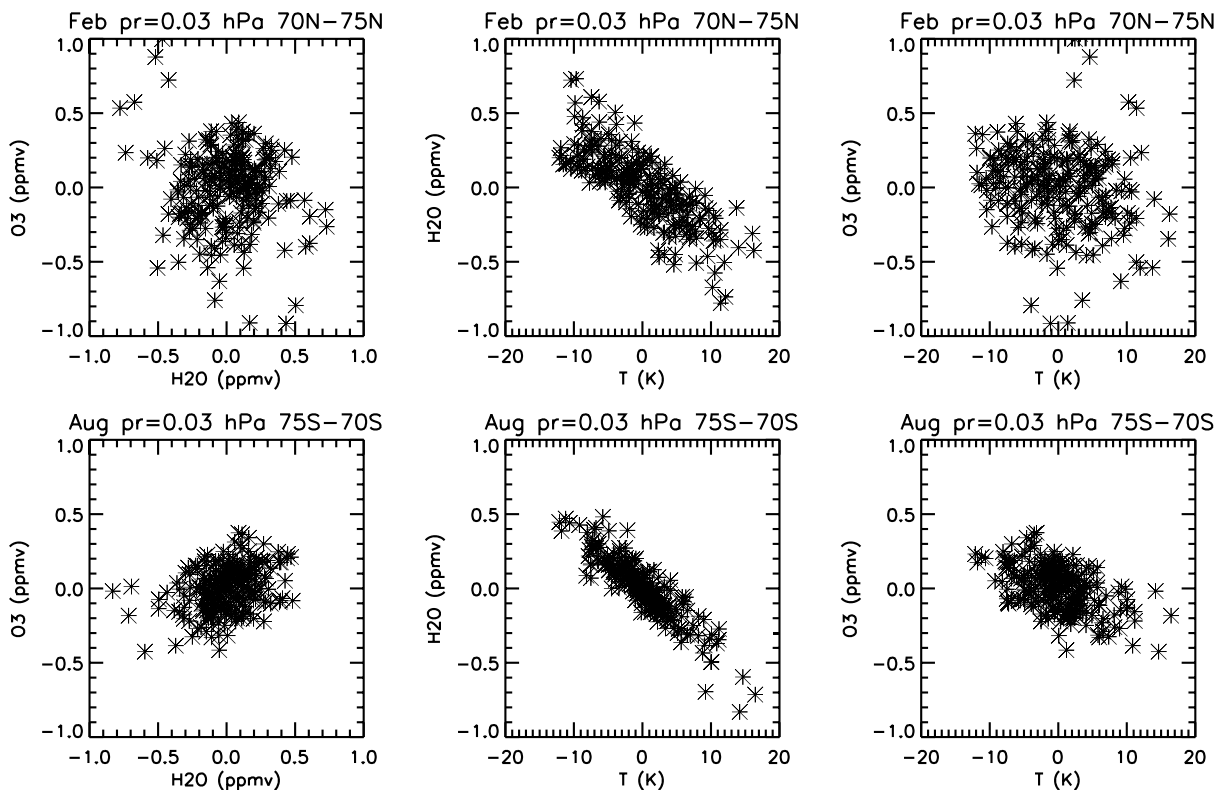
**Figure 13.** Scatter plots of the monthly average perturbations from the zonal average of nighttime ozone vmr versus $H_2O$ vmr, $H_2O$ vmr versus temperature, and ozone vmr versus temperature for the latitude bands 70°–75°N in the month of February (top) and 70°–75°S in the month of August (bottom). The points in each panel include 18 longitude bins over 13 years.

$O_3$ loss rate. The perturbation in ozone extends both poleward and equatorward of the terminator following the net airflow. At other longitudes, planetary wave motion gives poleward transport of midlatitude air with higher $H_2O$, leading to enhanced HOx production and depressed $O_3$ concentrations. The result is a strong wave structure in the ozone near the terminator and higher levels of $O_3$ toward the pole. In the southern hemisphere, the weaker dynamics reduces this planetary wave transport and results in only a weak longitudinal structure of the $O_3$, whose overall concentrations are lower.

## 4. Summary and Discussion

In this study, we combine observations from several sources to construct a multidimensional picture of the tertiary maximum in ozone in the winter mesosphere. The results confirm the presence of the ozone maximum in the polar winter middle mesosphere reported in several previous studies (e.g., Daae et al., 2014; Hartogh et al., 2004; Marsh et al., 2001; Sofieva et al., 2009, 2012). The observations provide new information about the structure and variability of mesospheric ozone in both hemispheres and over more than a decade of observations. The emphasis in this analysis is on monthly average nighttime ozone.

- In both hemispheres the location of maximum nighttime ozone moves with the season. Shortly after the autumn equinox and before the spring equinox, the highest ozone vmr is seen near the pole. The location of the maximum shifts to about 70° latitude near the solstice. In the SH, the pressure of the maximum ozone is lower (altitude is higher) in the early and late winter periods, while in the NH, the maximum ozone is at lower altitude in late winter.
- The seasonal variations in high-latitude ozone are affected by variations in the concentration of $H_2O$ over the polar cap. The maximum ozone vmr is large where the $H_2O$ vmr is very low. The lowest concentrations of $H_2O$ occur in the polar region of the NH late winter during elevated stratopause events.

- Overall, the ozone vmr at the tertiary maximum in the NH is higher than that in the SH. The hemispheric differences are seen even when comparing SH winters to only those NH winters that do not have an elevated stratopause event.
- The maximum ozone has strong longitudinal variations in the presence of large quasi-stationary planetary waves in the NH. These variations are seen in latitudes that are equatorward of the polar night terminator. They are due to variations in temperature and $H_2O$.

Beginning with the investigation of Marsh et al. (2001), previous studies have noted how seasonal variations in the radiative environment affect the ozone. In particular, the reduced photolysis of $H_2O$ to generate HOx was shown to account for the season and latitude of the maximum. Several investigations (e.g., Damiani et al., 2010; Smith et al., 2009; Sonnemann et al., 2006; Tweedy et al., 2013) highlighted the interannual variability of ozone in response to variable dynamics in NH winters. In this study, we find that the vertical transport of HOx, the abundance of $H_2O$, and the temperature are all factors in controlling interannual variations and differences between the two hemispheres. The dynamical influence is seen in two components: (1) the overall lower $H_2O$ and higher temperature in the NH polar cap due to more vigorous downwelling associated with dynamical disturbances and (2) the importance of low $H_2O$ air in the polar region and its transport equatorward by planetary waves. Consistent with the roles of the mean circulation and transport by planetary waves, air with low $H_2O$ tends to also have higher temperature. The impacts of $H_2O$ and temperature perturbations tend to partially cancel; the low HOx resulting from low $H_2O$ gives a tendency for higher ozone while simultaneous higher temperature gives a tendency for lower equilibrium nighttime ozone.

The $H_2O$ and temperature perturbations associated with the mean circulation and with quasi-stationary planetary waves are not entirely independent. The planetary waves that transport low $H_2O$ air horizontally into lower latitudes also contribute to driving the mean circulation that brings down low $H_2O$ air from the upper mesosphere (e.g., Limpasuvan et al., 2016). However, the primary driver of the downwelling component of the circulation at this altitude is believed to be gravity waves (e.g., Siskind et al., 2007). There is an interplay between the planetary waves and gravity waves that cannot be readily diagnosed from the mean concentration of $H_2O$ or the presence of planetary waves.

## References

Chandran, A., Collins, R. L., Garcia, R. R., Marsh, D. R., Harvey, V. L., Yue, J., & de la Torre, L. (2013). A climatology of elevated stratopause events in the Whole Atmosphere Community Climate Model. *Journal of Geophysical Research: Atmospheres*, 118, 1234–1246. https://doi.org/10.1002/jgrd.50123

Daae, M., Espy, P., Nesse Tyssøy, H., Newnham, D., Stadsnes, J., & Søraas, F. (2012). The effect of energetic electron precipitation on middle mesospheric night-time ozone during and after a moderate geomagnetic storm. *Geophysical Research Letters*, 39, L21811. https://doi.org/10.1029/2012GL053787

Daae, M., Straub, C., Espy, P. J., & Newnham, D. A. (2014). Atmospheric ozone above Troll station, Antarctica observed by a ground based microwave radiometer. *Earth System Science Data*, 6(1), 105–115. https://doi.org/10.5194/essd-6-105-2014

Damiani, A., Storini, M., Santee, M. L., & Wang, S. (2010). Variability of the nighttime OH layer and mesospheric ozone at high latitudes during northern winter: Influence of meteorology. *Atmospheric Chemistry and Physics*, 10(21), 10,291–10,303. https://doi.org/10.5194/acp-10-10291-2010

Forkman, P., Eriksson, P., Murtagh, D., & Espy, P. (2005). Observing the vertical branch of the mesospheric circulation at latitude 60°N using ground-based measurements of CO and $H_2O$. *Journal of Geophysical Research*, 110, D05107. https://doi.org/10.1029/2004JD004916

Froidevaux, L., Jiang, Y. B., Lambert, A., Livesey, N. J., Read, W. G., Waters, J. W., et al. (2008). Validation of Aura Microwave Limb Sounder stratospheric ozone measurements. *Journal of Geophysical Research*, 113, D15S20. https://doi.org/10.1029/2007JD008771

Hartogh, P., Jarchow, C., Sonnemann, G. R., & Grygalashvyly, M. (2004). On the spatiotemporal behavior of ozone within the upper mesosphere/mesopause region under nearly polar night conditions. *Journal of Geophysical Research*, 109, D18303. https://doi.org/10.1029/2004JD004576

Hartogh, P., Jarchow, C., Sonnemann, G. R., & Grygalashvyly, M. (2011). Ozone distribution in the middle latitude mesosphere as derived from microwave measurements at Lindau (51.66°N, 10.13°E). *Journal of Geophysical Research*, 116, D04305. https://doi.org/10.1029/2010JD014393

Kvissel, O.-K., Orsolini, Y. J., Stordal, F., Limpasuvan, V., Richter, J., & Marsh, D. R. (2012). Mesospheric intrusion and anomalous chemistry during and after a major stratospheric sudden warming. *Journal of Atmospheric and Solar: Terrestrial Physics*, 78-79, 116–124. https://doi.org/10.1016/j.jastp.2011.08.015

Limpasuvan, V., Orsolini, Y. J., Chandran, A., Garcia, R. R., & Smith, A. K. (2016). On the composite response of the MLT to major sudden stratospheric warming events with elevated stratopause. *Journal of Geophysical Research: Atmospheres*, 121, 4518–4537. https://doi.org/10.1002/2015JD024401

Livesey, N. J., Read, W. G., Wagner, P. A., Froidevaux, L., Lambert, A., Manney, G. L., et al. (2017). Earth Observing System (EOS) Aura Microwave Limb Sounder (MLS) Version 4.2x Level 2 data quality and description document (JPL Tech. Rep. JPL D-33509 Rev. C, 169 pp.). Retrieved from https://mls.jpl.nasa.gov/data/v4-2_data_quality_document.pdf

López-Puertas, M., García-Comas, M., Funke, B., Gardini, A., Stiller, G. P., von Clarmann, T., et al. (2018). MIPAS observations of ozone in the middle atmosphere. *Atmospheric Measurement Techniques Discussions*, 1–35. https://doi.org/10.5194/amt-2017-467

Manney, G. L., Schwartz, M. J., Krüger, K., Santee, M. L., Pawson, S., Lee, J. N., et al. (2009). Aura Microwave Limb Sounder observations of dynamics and transport during the record-breaking 2009 Arctic stratospheric major warming. *Geophysical Research Letters*, *36*, L12815. https://doi.org/10.1029/2009GL038586

Marsh, D., Smith, A., & Noble, E. (2003). Mesospheric ozone response to changes in water vapor. *Journal of Geophysical Research*, *108*(D3), 4109. https://doi.org/10.1029/2002JD002705

Marsh, D. R., Smith, A. K., Brasseur, G., Kaufmann, G. M., & Grossmann, K. (2001). The existence of a tertiary ozone maximum in the high-latitude middle mesosphere. *Geophysical Research Letters*, *28*(24), 4531–4534. https://doi.org/10.1029/2001GL013791

Morgenstern, O., Hegglin, M. I., Rozanov, E., O'Connor, F. M., Abraham, N. L., Akiyoshi, H., et al. (2017). Review of the global models used within phase 1 of the Chemistry–Climate Model Initiative (CCMI). *Geoscientific Model Development*, *10*(2), 639–671. https://doi.org/10.5194/gmd-10-639-2017.

Muscari, G., Cesaroni, C., Fiorucci, I., Smith, A. K., Froidevaux, L., & Mlynczak, M. G. (2012). Strato-mesospheric ozone measurements using ground-based millimeter-wave spectroscopy at Thule, Greenland. *Journal of Geophysical Research*, *117*, D07307. https://doi.org/10.1029/2011JD016863

Orsolini, Y. J., Urban, J., Murtagh, D. P., Lossow, S., & Limpasuvan, V. (2010). Descent from the polar mesosphere and anomalously high stratopause observed in 8 years of water vapor and temperature satellite observations by the Odin Sub-Millimeter Radiometer. *Journal of Geophysical Research*, *115*, D12305. https://doi.org/10.1029/2009JD013501

Pickett, H. M., Drouin, B. J., Canty, T., Salawitch, R. J., Fuller, R. A., Perun, V. S., et al. (2008). Validation of Aura Microwave Limb Sounder OH and $HO_2$ measurements. *Journal of Geophysical Research*, *113*, D16S30. https://doi.org/10.1029/2007JD008775

Russell, J. M. III, Bailey, S. M., Gordley, L. L., Rusch, D. W., Horányi, M., Hervig, M. E., et al. (2009). Aeronomy of Ice in the Mesosphere (AIM): Overview and early science results. *Journal of Atmospheric and Solar: Terrestrial Physics*, *71*(3-4), 289–299. https://doi.org/10.1016/j.jastp.2008.08.011

Seppälä, A., Verronen, P. T., Sofieva, V. F., Tamminen, J., Kyrola, E., Rodger, C. J., & Clilverd, M. A. (2006). Destruction of the tertiary ozone maximum during a solar proton event. *Geophysical Research Letters*, *33*, L07804. https://doi.org/10.1029/2005GL025571

Siskind, D. E., Eckermann, S. D., Coy, L., McCormack, J. P., & Randall, C. E. (2007). On recent interannual variability of the Arctic winter mesosphere: Implications for tracer descent. *Geophysical Research Letters*, *34*, L09806. https://doi.org/10.1029/2007GL029293

Smith, A. K., Harvey, V. L., Mlynczak, M. G., Funke, B., García-Comas, M., Hervig, M., et al. (2013). Satellite observations of ozone in the upper mesosphere. *Journal of Geophysical Research: Atmospheres*, *118*, 5803–5821. https://doi.org/10.1002/jgrd.50445

Smith, A. K., Lopez-Puertas, M., Garcia-Comas, M., & Tukiainen, S. (2009). SABER observations of mesospheric ozone during NH late winter 2002–2009. *Geophysical Research Letters*, *36*, L23804. https://doi.org/10.1029/2009GL040942

Smith, A. K., & Marsh, D. R. (2005). Processes that account for the ozone maximum at the mesopause. *Journal of Geophysical Research*, *110*, D23305. https://doi.org/10.1029/2005JD006298

Smith, A. K., Marsh, D. R., Mlynczak, M. G., & Mast, J. C. (2010). Temporal variations of atomic oxygen in the upper mesosphere from SABER. *Journal of Geophysical Research*, *115*, D18309. https://doi.org/10.1029/2009JD013434

Sofieva, V. F., Kalakoski, N., Verronen, P. T., Päivärinta, S.-M., Kyrölä, E., Backman, L., & Tamminen, J. (2012). Polar-night $O_3$, $NO_2$ and $NO_3$ distributions during sudden stratospheric warmings in 2003–2008 as seen by GOMOS/Envisat. *Atmospheric Chemistry and Physics*, *12*(2), 1051–1066. https://doi.org/10.5194/acp-12-1051-2012

Sofieva, V. F., Kyrölä, E., Verronen, P. T., Seppälä, A., Tamminen, J., Marsh, D. R., et al. (2009). Spatio-temporal observations of the tertiary ozone maximum. *Atmospheric Chemistry and Physics*, *9*(13), 4439–4445. https://doi.org/10.5194/acp-9-4439-2009

Sonnemann, G. R., Grygalashvyly, M., & Berger, U. (2006). Impact of a stratospheric warming event in January 2001 on the minor constituents in the MLT region calculated on the basis of a new 3D-model LIMA of the dynamics and chemistry of the middle atmosphere. *Journal of Atmospheric and Solar: Terrestrial Physics*, *68*(17), 2012–2025. https://doi.org/10.1016/j.jastp.2006.04.005

Sonnemann, G. R., Hartogh, P., Grygalashvyly, M., Li, S., & Berger, U. (2008). The quasi 5-day signal in the mesospheric water vapor concentration at high latitudes in 2003-a comparison between observations at ALOMAR and calculations. *Journal of Geophysical Research*, *113*, D04101. https://doi.org/10.1029/2007JD008875

Turunen, E., Kero, A., Verronen, P. T., Miyoshi, Y., Oyama, S.-I., & Saito, S. (2016). Mesospheric ozone destruction by high-energy electron precipitation associated with pulsating aurora. *Journal of Geophysical Research: Atmospheres*, *121*, 11,852–11,861. https://doi.org/10.1002/2016JD025015

Tweedy, O. V., Limpasuvan, V., Orsolini, Y. J., Smith, A. K., Garcia, R. R., Kinnison, D., et al. (2013). Nighttime secondary ozone layer during major stratospheric sudden warmings in specified-dynamics WACCM. *Journal of Geophysical Research: Atmospheres*, *118*, 8346–8358. https://doi.org/10.1002/jgrd.50651

Verronen, P. T., Seppälä, A., Kyrölä, E., Tamminen, J., Pickett, H. M., & Turunen, E. (2006). Production of odd hydrogen in the mesosphere during the January 2005 solar proton event. *Geophysical Research Letters*, *33*, L24811. https://doi.org/10.1029/2006GL028115

von Clarmann, T., Funke, B., López-Puertas, M., Kellmann, S., Linden, A., Stiller, G. P., et al. (2013). The solar proton events in 2012 as observed by MIPAS. *Geophysical Research Letters*, *40*, 2339–2343. https://doi.org/10.1002/grl.50119

Zawedde, A. E., Nesse Tyssøy, H., Hibbins, R., Espy, P. J., Ødegaard, L.-K., Sandanger, M. I., & Stadsnes, J. (2016). The impact of energetic Electron precipitation on mesospheric hydroxyl during a year of solar minimum. *Journal of Geophysical Research: Space Physics*, *121*, 5914–5929. https://doi.org/10.1002/2016JA022371